

# Two-dimensional hyperbolic phonon polariton waveguide: an analytical model and scanning near-field optical microscopy studies

Fengsheng Sun<sup>1,†</sup>, Wuchao Huang<sup>1,†</sup>, Zebo Zheng<sup>1,†</sup>, Ningsheng Xu<sup>2</sup>, Runze Zhan<sup>1</sup>, Huanjun Chen<sup>1,\*</sup>, Shaozhi Deng<sup>1,\*</sup>

<sup>1</sup>*State Key Laboratory of Optoelectronic Materials and Technologies,  
Guangdong Province Key Laboratory of Display Material and Technology,  
School of Electronics and Information Technology,  
Sun Yat-sen University, Guangzhou 510275*

<sup>2</sup>*Fudan University, Shanghai 200433*

<sup>†</sup>*These authors contributed equally*

**Abstract:** We theoretically analyzed the propagation of the phonon polaritons (PhPs) of van der Waals (vdW)  $\alpha$ -MoO<sub>3</sub> biaxial crystal by solving the wave equation in two dimensional optical waveguide model. The dispersion relation and electromagnetic field distribution of different orders PhPs waves are obtained. And it is found that the in-plane spatial dispersion relations of  $\alpha$ -MoO<sub>3</sub> waveguide modes are elliptical and hyperbolical in different mid-infrared response bands. Using the near-field optical nanoimaging, we obtain the directly experimental evidence for the in-plane dispersion of  $\alpha$ -MoO<sub>3</sub> waveguide modes, which support our theoretical prediction.

The phenomenon of optical birefringence indicates that the crystal is optically anisotropic and has different properties for different polarized light. This special optical property of crystal is the result of interaction between electromagnetic field and crystal, which shows the anisotropy of interaction between crystal and electromagnetic field. The anisotropic crystal will polarize under the action of the external electromagnetic field. If the material structure is anisotropic, the polarization of the material is also anisotropic [1]. Due to the novel properties of anisotropic materials, the artificial design and construction of metamaterials have attracted great attention. Van der Waals (VdW) materials is a kind of natural anisotropic material [2, 3]. Compared with the artificial anisotropic materials, the natural anisotropic materials provide the uniformity of materials in a smaller scale. Such vdW materials and atoms between layers are bonded by a weak vdW force, and atoms in unit layer are covalently bonded. The bonding mode of vdW materials determines that such materials can cause highly anisotropic lattice vibrations along different crystal directions. This also leads to the anisotropic optical response of vdW materials. When the element in the dielectric tensor which describing the optical response has a different sign, the material exhibits novel hyperbolic response characteristics. So far, it has been found that hyperbolic response vdW materials are hexagonal boron nitride [4–8] (*h*-BN) and  $\alpha$  phase molybdenum oxide [9–11] ( $\alpha$ -MoO<sub>3</sub>). Where *h*-BN is a natural uniaxial hyperbolic material, and  $\alpha$ -MoO<sub>3</sub> is a kind of natural biaxial hyperbolic material.

Polaritons are electromagnetic waves coupled to charged dipoles in solid-state materials [12]. Due to the different mechanism of material and electromagnetic field, the kinds of polaritons are complex [2, 3]. These include surface plasmons polaritons [13–17] (SPPs),

phonon polaritons [4–11] (PhPs) and exciton polaritons [18–20](EPs). Recently, it has been found that vdW crystal is a 2D material which can support the transmission of polaritons. Where PhPs induced by coupling of electromagnetic fields with optical phonons in polar crystals which can strongly confine the free-space light field deeply below the subwavelength region. PhPs have been studied in various polar dielectric crystals, and the propagation of PhPs can be modulated by heterostructure [7, 8] and metasurface [21]. The propagation of polaritons has became the focus of attention, but the analytical solution which can describe the propagation of polaritons in 2D materials completely has not been reported.

In this letter, we obtain the analytical solution describing the propagation evolution of the PhPs by solving the Maxwell's equations in 2D optical flake waveguide model. This is an important part of the study of polaritons propagation. It shows that PhPs waves are transverse magnetic (TM) waveguide modes, and the dispersion relations of TM modes and the spatial distribution of electromagnetic field are obtained. The unpublished works [22] without experimental verification are similar to ours. Taking  $\alpha$ -MoO<sub>3</sub> as an example, we obtained the elliptical and hyperbolic in-plane spatial dispersion at different excitation frequencies. In order to verify the correctness of the theoretical model, the numerical solution is obtained by numerical simulation with COMSOL software. In order to show the in-plane spatial dispersion of  $\alpha$ -MoO<sub>3</sub>, the near-field optical scanning of its circular hole nanostructures was carried out. This latter provides a theoretical support and an effective experimental method for studying the propagation evolution of PhPs. Due to the pulse in the waveguide is the linear superposition of the regular modes of the waveguide in narrow band, the theoretical analysis also lays the foundation for the pulse propagation in the 2D optical flake waveguide.

\* E-mail: chenhj8@mail.sysu.edu.cn;stsdzs@mail.sysu.edu.cn

In order to investigate the propagation characteristics of PhPs, the propagation model of 2D optical flake

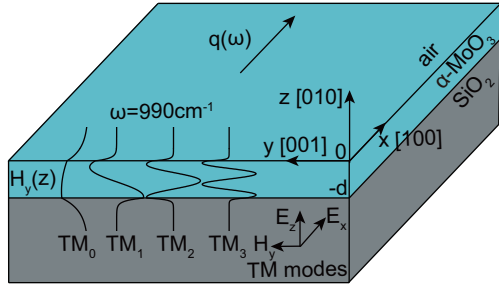


FIG. 1. Schematic diagram of three-layer optical flake waveguide.

waveguide needs to be established. In the coordinate system aligned to axis of a anisotropic crystal, the optical properties of biaxial bulk materials can be expressed by dielectric permittivity tensor  $\hat{\varepsilon}$  can be expressed as

$$\hat{\varepsilon} = \begin{pmatrix} \varepsilon_x & 0 & 0 \\ 0 & \varepsilon_y & 0 \\ 0 & 0 & \varepsilon_z \end{pmatrix}, \quad (1)$$

when the element in the dielectric tensor has a negative value, the waveguide just can support the propagation of transverse magnetic (TM) modes [2, 3]. It is assumed that the substrate and the covering are isotropic materials, and their dielectric constants are  $\varepsilon_s$  and  $\varepsilon_c$  respectively. Let's first assume that the electromagnetic wave travels along the x-axis, and the corresponding transmitted waveguide modes can be expressed as  $\mathbf{E}(x, z) = \vec{e}E(z)\exp(iqx - i\omega t)$ . TM modes ( $E_x, H_y, E_z$ ) in the 2D flake waveguide just have a magnetic field component  $H_y$  which polarized along y-axis, which is coupled by Maxwell's equations to an electric field in the x-z plane having both  $E_x$  and  $E_z$  components. The equations describing the magnetic field strength in each medium are

$$\begin{cases} \frac{\partial^2 H_y}{\partial^2 z} + (k_0^2 \varepsilon_{c,s} - q^2) H_y = 0, \\ \frac{\partial^2 H_y}{\partial^2 z} + (k_0^2 \varepsilon_x - \frac{\varepsilon_x}{\varepsilon_z} q^2) H_y = 0, \end{cases} \quad (2)$$

where  $k_0 = 2\pi/\lambda$  is the free space wavevector,  $q$  is the propagation constant of TM modes. The waveguide modes are bounded solution of bound state, so it must satisfy  $k_0^2 \varepsilon_{c,s} - q^2 < 0$  and  $k_0^2 \varepsilon_x - (\varepsilon_x/\varepsilon_z) q^2 > 0$ . The bound state solutions of the equations (2) describing the magnetic field distribution in the cover layer ( $z > 0$ ), waveguide layer ( $-d < z < 0$ ) and substrate layer ( $z < -d$ ) which are displayed in Fig.1 are

$$H_y = \begin{cases} A \exp(-\alpha_c z), \\ A \cos(k_z z) + B \sin(k_z z), \\ [A \cos(k_z d) - B \sin(k_z d)] \exp[\alpha_s(z + d)], \end{cases} \quad (3)$$

where  $\alpha_{c,s} = \sqrt{q^2 - k_0^2 \varepsilon_{c,s}}$ ,  $k_z = \sqrt{k_0^2 \varepsilon_x - (\varepsilon_x/\varepsilon_z) q^2}$  and  $d$  is the thickness of the optical flake waveguide. Using

the Faraday's law  $\nabla \times \mathbf{H} = i\omega \hat{\varepsilon} \mathbf{E}$ , we can get the distribution of electric fields component  $E_x$  which parallel to waveguide surface are

$$E_x = \begin{cases} -\frac{i\alpha_c}{\omega \varepsilon_0 \varepsilon_c} A \exp(-\alpha_c z), \\ -\frac{ik_z}{\omega \varepsilon_0 \varepsilon_x} [A \sin(k_z z) - B \cos(k_z z)], \\ \frac{i\alpha_s}{\omega \varepsilon_0 \varepsilon_s} [A \cos(k_z d) - B \sin(k_z d)] \exp[\alpha_s(z + d)], \end{cases} \quad (4)$$

and electric fields component  $E_z$  which perpendicular to waveguide surface are

$$E_z = \begin{cases} \frac{q}{\omega \varepsilon_0 \varepsilon_c} A \exp(-\alpha_c z), \\ \frac{q}{\omega \varepsilon_0 \varepsilon_x} [A \sin(k_z z) - B \cos(k_z z)], \\ \frac{q}{\omega \varepsilon_0 \varepsilon_s} [A \cos(k_z d) - B \sin(k_z d)] \exp[\alpha_s(z + d)], \end{cases} \quad (5)$$

Next, we need to match the continuity boundary condition of electromagnetic field at the interface ( $z = 0, -d$ ) of different medium

$$\begin{cases} E_{xc} = E_{xw}, & H_{yc} = H_{yw} \quad (z = 0), \\ E_{xw} = E_{xs}, & H_{yw} = H_{ys} \quad (z = -d), \end{cases} \quad (6)$$

then we can get

$$\begin{pmatrix} \frac{\alpha_c}{\varepsilon_c} \\ \frac{k_z}{\varepsilon_x} \sin(k_z d) - \frac{\alpha_s}{\varepsilon_s} \cos(k_z d) & \frac{k_z}{\varepsilon_x} \cos(k_z d) + \frac{\alpha_s}{\varepsilon_s} \sin(k_z d) \end{pmatrix} \begin{pmatrix} A \\ B \end{pmatrix} = 0. \quad (7)$$

The equations (7) have nontrivial solutions just when determinant is zero, then the dispersion relation of TM modes in optical flake waveguide is obtained which expressed as

$$k_z d = \arctan\left(\frac{\sqrt{\varepsilon_x \varepsilon_z}}{\varepsilon_c} \frac{\alpha_c}{k_z}\right) + \arctan\left(\frac{\sqrt{\varepsilon_x \varepsilon_z}}{\varepsilon_s} \frac{\alpha_s}{k_z}\right) + m\pi \quad (8)$$

Without loss of generality, when the propagation direction of waveguide modes is in any direction of in-plane, coordinate transformation is needed to study the optical propagation in non-spindle coordinate system. Coordinate matrix of the principal axis coordinate system is expressed as  $\hat{X} = (x, y, z)^T$ . If the transformation matrix is expressed as  $\hat{T}$ , then coordinate matrix and dielectric tensor in the non principal axis coordinate system can be expressed as  $\hat{X}' = \hat{T} \hat{X} = (x', y', z')^T$  and  $\hat{\varepsilon}' = \hat{T} \hat{\varepsilon} \hat{T}^{-1}$ , respectively. The corresponding electromagnetic field component of TM modes propagating in  $x'$  direction is  $(E_{x'}, H_{y'}, E_{z'})$ . In order to discuss the propagation of anisotropic flake waveguide modes in non-spindle axis direction, the rotation transformation matrix  $\hat{T}$  can be expressed as

$$\hat{T} = \begin{pmatrix} \cos \theta & \sin \theta & 0 \\ -\sin \theta & \cos \theta & 0 \\ 0 & 0 & 1 \end{pmatrix}, \quad (9)$$

and the dielectric tensor  $\hat{\varepsilon}'$  can be expressed as

$$\hat{\varepsilon}' = \begin{pmatrix} \varepsilon_x \cos^2 \theta + \varepsilon_y \sin^2 \theta & (\varepsilon_y - \varepsilon_x) \sin \theta \cos \theta & 0 \\ (\varepsilon_y - \varepsilon_x) \sin \theta \cos \theta & \varepsilon_x \cos^2 \theta + \varepsilon_y \sin^2 \theta & 0 \\ 0 & 0 & 1 \end{pmatrix}. \quad (10)$$

Order  $\varepsilon_t = \varepsilon_x \cos^2 \theta + \varepsilon_y \sin^2 \theta$ , the dispersion relations under the non-spindle coordinate system can be expressed as

$$\begin{aligned} \sqrt{\frac{\varepsilon_t}{\varepsilon_z}} \sqrt{k_0^2 \varepsilon_z - q^2} d = \tan^{-1} \left( \frac{\sqrt{\varepsilon_t \varepsilon_z}}{\varepsilon_c} \sqrt{\frac{q^2 - k_0^2 \varepsilon_c}{k_0^2 \varepsilon_z - q^2}} \right) \\ + \tan^{-1} \left( \frac{\sqrt{\varepsilon_t \varepsilon_z}}{\varepsilon_s} \sqrt{\frac{q^2 - k_0^2 \varepsilon_s}{k_0^2 \varepsilon_z - q^2}} \right) + m\pi, \end{aligned} \quad (11)$$

where  $m = 0, 1, 2 \dots$  is the order of TM modes. The equation (11) implies that the relation  $q[\hat{\varepsilon}(\omega), d, \theta, m]$ . This is the analytical formula of dispersion relation of waveguide modes. Our theoretical model is Maxwell's equations, now we make transformations as follows

$$\bar{x} = \frac{x}{\kappa}, \bar{y} = \frac{y}{\kappa}, \bar{z} = \frac{z}{\kappa}. \quad (12)$$

Before and after the transformation, only the scale has changed, the system of Maxwell's equations keep unchanged. The TM modes which considered owns the transform invariance. For simplicity, the parameters of the waveguide models before and after the transformation can be expressed as

$$\begin{aligned} \Sigma_1 &= \{\psi(x, y, z, t), k_0, k_z, \alpha_c, \alpha_s, q\}, \\ \bar{\Sigma}_2 &= \{\bar{\psi}(\bar{x}, \bar{y}, \bar{z}, t), \kappa k_0, \kappa k_z, \kappa \alpha_c, \kappa \alpha_s, \kappa q\}, \end{aligned} \quad (13)$$

where  $\psi(x, y, z, t)$  represents the temporal and spatial distribution of electromagnetic field in propagation modes. If  $\kappa$  has dimension of length, the transformed system is dimensionless. So the influence of sample thickness  $d$  on dispersion relation is eliminated when  $\kappa = d$ .

Different kinds of polaritons in optical waveguides come from different kinds of particles coupled with electromagnetic field. In vdWs crystal,  $h$ -BN and  $\alpha$ -MoO<sub>3</sub> are hyperbolic materials that can support the propagation of PhPs which based on crystalline structure. The optical response of the polar vdWs crystal is dominated by the phonon absorption, and its dielectric tensor can be calculated by using a Lorentz model [5, 6, 11] :

$$\varepsilon_j(\omega) = \varepsilon_\infty^j \left( 1 + \frac{\omega_{LO}^{j2} - \omega_{TO}^{j2}}{\omega_{TO}^{j2} - \omega^2 - i\omega\Gamma_j} \right), \quad (j = x, y, z) \quad (14)$$

where  $\varepsilon_j$  denotes the diagonal element in the dielectric tensor of the spindle. The parameter  $\varepsilon_\infty^j$  is the high frequency dielectric constant, parameters  $\omega_{LO}$  and  $\omega_{TO}$  are longitudinal optical (LO) and transverse optical (TO) phonon frequencies, respectively. And  $\Gamma$  is the broadening factor. In vdWs crystal,  $h$ -BN and  $\alpha$ -MoO<sub>3</sub> are materials that can support the propagation of PhPs which

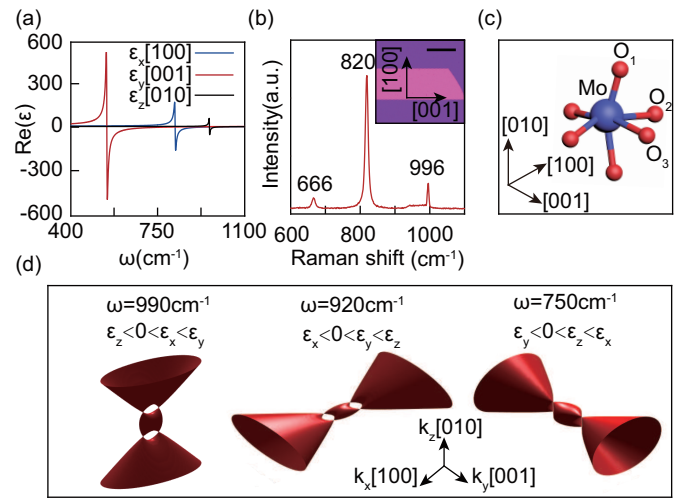


FIG. 2. Optical properties and lattice structure of  $\alpha$ -MoO<sub>3</sub>. (a) Dielectric constant of  $\alpha$ -MoO<sub>3</sub>. (b) Raman spectrum of  $\alpha$ -MoO<sub>3</sub> in illustration. Scale bars=200 $\mu$ m. (c) Crystalline structure of  $\alpha$ -MoO<sub>3</sub>. (d) Iso-frequency surfaces of  $\alpha$ -MoO<sub>3</sub>.

based on crystalline structure.  $\alpha$ -MoO<sub>3</sub> is taken as an example in this latter, which is a natural biaxial hyperbolic material. These parameters of  $\alpha$ -MoO<sub>3</sub> in this paper were taken from the existing literature [11]. Fig.2 (b) is the Raman spectrum of  $\alpha$ -MoO<sub>3</sub>. Due to the different infrared activity of phonon modes along different crystalline directions, the infrared response range of phonons in different crystalline directions is also different which shows in Fig.2 (c). In the Reststrahlen band between the LO and TO frequencies of phonon response, the real part of dielectric constant  $Re(\varepsilon_j)$  is negative. Fig.2 (a) shows the dielectric constant of  $\alpha$ -MoO<sub>3</sub>. In the spindle coordinate system, the x, y and z-axis which correspond to the crystalline directions [100], [001], and [010] of the  $\alpha$ -MoO<sub>3</sub>, respectively. The optical properties of bulk materials can be described by iso-frequency surfaces [23], which describes the material dispersion by the wave vector of plane electromagnetic wave. And the iso-frequency surfaces can be calculated by

$$\begin{aligned} (\varepsilon_x k_x^2 + \varepsilon_y k_y^2 + \varepsilon_z k_z^2)(k_x^2 + k_y^2 + k_z^2) + k_0^4 \varepsilon_x \varepsilon_y \varepsilon_z \\ - k_0^2 [\varepsilon_x (\varepsilon_y + \varepsilon_z) k_x^2 + \varepsilon_y (\varepsilon_x + \varepsilon_z) k_y^2 + \varepsilon_z (\varepsilon_x + \varepsilon_y) k_z^2] = 0. \end{aligned} \quad (15)$$

Fig.2 (d) shows the iso-frequency surfaces of  $\alpha$ -MoO<sub>3</sub> at frequencies  $990\text{cm}^{-1}$ ,  $920\text{cm}^{-1}$  and  $750\text{cm}^{-1}$ , respectively. And the optical hyperbolic response characteristics are shown in different frequency bands.

The propagation characteristics of waveguide modes are determined by material dispersion and the spatial structure of waveguide. In the past, the Fresnel reflection coefficient  $r_p$  [4, 7, 8, 10, 11, 13, 24] has been used to calculate the dispersion relation of 2D optical waveguide. But this method can only rough calculate the dispersion relation and can't describe the evolution of electromag-

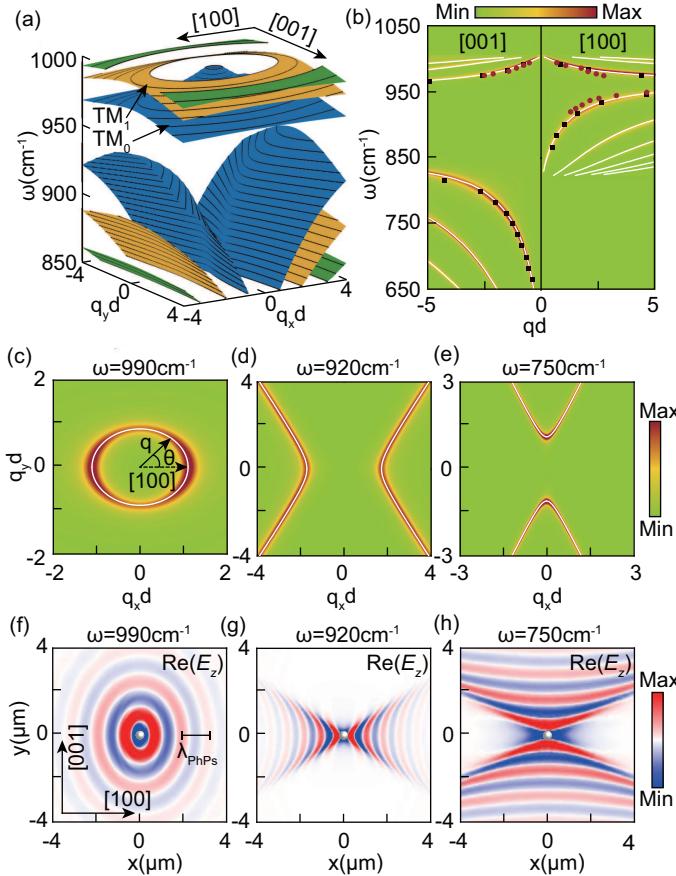


FIG. 3. Dispersion relation and electromagnetic field distribution of  $\alpha$ -MoO<sub>3</sub> flake waveguide modes. (a) Dispersion relation for the PhPs in  $\alpha$ -MoO<sub>3</sub> waveguide. (b) Dispersion relation of  $\alpha$ -MoO<sub>3</sub> waveguide modes along [100] and [001] directions. (c-e) In-plane spatial dispersion of PhPs at three specific frequency. (f-h) Calculated  $\text{Re}(E_z)$  of electric field distributions launching with a p-polarized electric dipole. The false color image in (b-e) reflects the imaginary part of the complex reflectivity,  $\text{Im}r_p$ , of the air/ $\alpha$ -MoO<sub>3</sub>/SiO<sub>2</sub> multilayer structure. The white solid line in (b-e) is the analytical results. In (b), the black square and the red circle are the numerical results and experimental data respectively.

netic fields completely. In order to show the superiority of the analytical solution, the comparison between the dispersion relation calculated by Fresnel reflection coefficient and the results calculated by the analytical solution (11) is shown in Fig.3 (b-e). And in Fig.1, we draw the magnetic field  $H_y$  distribution curve of several order waveguide modes which are propagating along the [100] crystal direction when the excitation frequency is  $990\text{cm}^{-1}$ . This can not be achieved by Fresnel reflection coefficient. Fig.3 (a) is the dispersion relation at mid-infrared frequency band of air/ $\alpha$ -MoO<sub>3</sub>/SiO<sub>2</sub> multilayer structure. At the same excitation frequency, the propagation constant  $q$  of the mode increases with the increase of waveguide mode order  $m$ . The contour in Fig.3 (a) is the in-plane spatial dispersion at the corresponding

frequency. The in-plane spatial dispersion reflects the propagation behavior of waveguide modes in different directions. Fig.3 (c-e) shows the in-plane spatial dispersion of TM<sub>0</sub> mode at frequencies  $990\text{cm}^{-1}$ ,  $920\text{cm}^{-1}$  and  $750\text{cm}^{-1}$ , respectively. There are two main kinds of in-plane spatial dispersion of  $\alpha$ -MoO<sub>3</sub> waveguide modes: elliptical and hyperbolic. The elliptical and hyperbolic in-plane spatial dispersion based on the out-plane ( $\varepsilon_z < 0$ ) and in-plane ( $\varepsilon_t < 0$ ) hyperbolic material dispersion of  $\alpha$ -MoO<sub>3</sub>. And they are in the abnormal dispersion region and the normal dispersion region respectively from Fig.3 (b). The in-plane spatial dispersion is equivalent to the Fourier transform of the in-plane distribution of electromagnetic field excited by a  $\vec{p}$ -dipole in Fig.3 (f-h). In order to consistent with the situation in experiments, the thickness  $d$  of  $\alpha$ -MoO<sub>3</sub> in the COMSOL numerical calculation is 210nm. And the statistics of numerical results of PhPs wavelength along [100] and [001] directions are displayed in Fig.3 (b). It can be found that the numerical solution and the analytical solution fit perfectly.

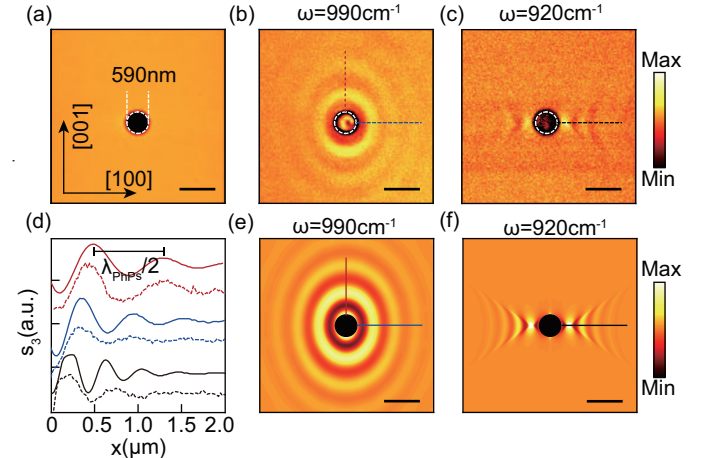


FIG. 4. Detection and analysis of PhPs in  $\alpha$ -MoO<sub>3</sub> microstructure. (a) AFM topography. (b-c) Near-field optical images of  $\alpha$ -MoO<sub>3</sub> circular hole microstructure. (d) Normalized near-field amplitudes at red, blue and black line marked in (b-c) and (d-e) respectively. (e-f) Theoretical interference patterns of the PhPs in  $\alpha$ -MoO<sub>3</sub>. Scale bars=1μm.

The in-plane propagation characteristics of PhPs can be observed by the way of nano antenna excitation in experiment, but this method requires the growth and transfer of metal nano particles. In order to show the propagation characteristics of the PhPs in  $\alpha$ -MoO<sub>3</sub> by a simple experimental method, the circular hole microstructure of  $\alpha$ -MoO<sub>3</sub> flakes was fabricated by electron beam lithography (EBL). Furthermore, the optical hyperbolic properties of  $\alpha$ -MoO<sub>3</sub> were studied by scanning near-field optical microscope (s-SNOM). Fig.4 (a) display the AFM image of a circular hole microstructure, then we can get the diameter of hole is 590nm and the thickness  $d$  of  $\alpha$ -MoO<sub>3</sub> flake is 210nm. Fig.4 (b) and (c) show the

near-field optical image of the circular hole with excitation frequencies of  $990\text{cm}^{-1}$  and  $920\text{cm}^{-1}$ , respectively. The hyperbolic response of  $\alpha\text{-MoO}_3$  is verified by this method. At the frequencies of  $990\text{cm}^{-1}$  and  $920\text{cm}^{-1}$ , the in-plane spatial dispersion of  $\alpha\text{-MoO}_3$  are elliptical and hyperbolic. The circular hole microstructure provides the reflection boundary for the PhPs excited by the AFM tip. The electric field without the circular hole microstructure were the sum of the tip launched PhPs and those reflected waves from the boundaries. In order to verify this experimental phenomenon, we theoretically calculate the electric field distribution which are displayed in Fig.4 (e-f) of the superposition of the PhPs excited by the AFM tip and reflected by the boundary of the circular hole, using the in-plane spatial dispersion in Fig.3 (c-d). The electromagnetic field after interference can be expressed as  $\psi = \psi_0 + \sum_j \psi_j$  [16, 17], where  $\psi_0$  is the PhPs wave lunched by AFM tip, and  $\psi_j = R_j \times \psi_0 \exp[-2q_j(\theta)r_j(\gamma + i)]$  are waves which reflected by the boundaries. Parameters  $R_j$ ,  $\gamma$  and  $r_i$  are reflection coefficient, damping rate and distance between the boundary and AFM tip. To simplify the analysis, we

just calculated interference of  $\text{TM}_0$  and fixed  $\psi_0$  and  $\gamma$  as 1 and 0.2 in the calculations, respectively. Fig 4(d) shows the comparison between the calculation and the experimental results along the [100] and [001] crystal directions of  $\alpha\text{-MoO}_3$  flake. The well matching between them proves the correctness of the theoretical flake waveguide model.

In conclusion, we explain the propagation of PhPs wave with the theory of 2D anisotropic flake waveguide model. Based on vdWs  $\alpha\text{-MoO}_3$  crystal, the dispersion relation and electromagnetic field distribution of the TM waveguide modes are calculated. And the numerical results are in good agreement with the analytical solution of the theory. Then the biaxial hyperbolic optical response of  $\alpha\text{-MoO}_3$  in mid-infrared band is reflected. The near-field optical scanning experiment of  $\alpha\text{-MoO}_3$  circle hole nanostructure demonstrated the biaxial hyperbolic optical properties of  $\alpha\text{-MoO}_3$  and verify the correctness of the theory. Furthermore, the theoretical model is verified to reveal the optical properties of waveguide materials. It provides a theoretical method for optical propagation in nanoscale.

---

[1] M. Born and E. Wolf. *Principles of Optics* 7th edn (London: Pergamon) (2005).

[2] T. Low, A. Chaves, J. D. Caldwell, A. Kumar, N. X. Fang, P. Avouris, T. F. Heinz, F. Guinea, L. Martin-Moreno, and F. Koppens. *Nat. Mater.* **16**, 182 (2016).

[3] D. N. Basov, M. M. Fogler, and F. J. García de Abajo. *Science* **354**, aag1992 (2016).

[4] S. Dai, Z. Fei, Q. Ma, A. S. Rodin, M. Wagner, A. S. McLeod, M. K. Liu, W. Gannett, W. Regan, K. Watanabe, T. Taniguchi, M. Thiemens, G. Dominguez, A. H. Castro Neto, A. Zettl, F. Keilmann, P. Jarillo-Herrero, M. M. Fogler, and D. N. Basov. *Science*, **343**, 1125 (2014).

[5] P. Li, I. Dolado, F. J. Alfaro-Mozaz, A. Yu. Nikitin, F. Casanova, L. E. Hueso, S. Vélez, and R. Hillenbrand. *Nano Lett.* **17**, 228 (2017).

[6] J. D. Caldwell, A. V. Kretinin, Y. G. Chen, V. Giannini, M. M. Fogler, Y. Francescato, C. T. Ellis, J. G. Tischler, C. R. Woods, A. J. Giles, M. Hong, K. Watanabe, T. Taniguchi, S. A. Maier, and K. S. Novoselov. *Nat. Commun.* **5**, 5221 (2014).

[7] A. Woessner, M. B. Lundeberg, Y. Gao, A. Principi, P. Alonso-Gonzlez, M. Carrega, K. Watanabe, T. Taniguchi, G. Vignale, M. Polini, J. Hone, R. Hillenbrand, and F. H. L. Koppens. *Nat. Mater.* **14**, 421 (2014).

[8] S. Dai, Q. Ma, M. K. Liu, T. Andersen, Z. Fei, M. D. Goldflam, M. Wagner, K. Watanabe, T. Taniguchi, M. Thiemens, F. Keilmann, G. C. A. M. Janssen, S-E. Zhu, P. Jarillo-Herrero, M. M. Fogler, and D. N. Basov. *Nat. Nanotechnol.* **10**, 682 (2015).

[9] W. Ma, P. Alonso-González, S. Li, A. Y. Nikitin, J. Yuan, J. Martín-Sánchez, J. Taboada-Gutiérrez, I. Amenabar, P. Li, S. Vélez, C. Tollar, Z. Dai, Y. Zhang, S. Sriram, K. Kalantar-Zadeh, S. Lee, R. Hillenbrand, and Q. Bao. *Nature* **562**, 557 (2018).

[10] Z. Zheng, J. Chen, Y. Wang, X. Wang, X. Chen, P. Liu, J. Xu, W. Xie, H. Chen, S. Deng, and N. Xu. *Adv. Mater.* **30**, 1705318 (2018).

[11] Z. Zheng, N. Xu, S. L. Oscurato, M. Tamagnone, F. Sun, Y. Jiang, Y. Ke, J. Chen, W. Huang, W. L. Wilson, A. Ambrosio, S. Deng, H. Chen. *Sci. Adv.* **5**, eaav8690 (2019).

[12] K. Huang, *Nature* **167**, 79 (1951).

[13] Z. Fei, G. O. Andreev, W. Bao, L.M. Zhang, A. S. McLeod, C. Wang, M. K. Stewart, Z. Zhao, G. Dominguez, M. Thiemens, Michael M. Fogler, Michael J. Tauber, A. H. Castro-Neto, C. N. Lau, F. Keilmann, and D. N. Basov. *Nano Lett.* **11**, 4701 (2011).

[14] Z. Fei, A. S. Rodin, G. O. Andreev, W. Bao, A. S. McLeod, M. Wagner, L.M. Zhang, Z. Zhao, M. Thiemens, G. Dominguez, Z. M. M. Fogler, A. H. Castro Neto, C. N. Lau, F. Keilmann and D. N. Basov, *Nature* **487**, 82 (2012).

[15] J. Chen, M. Badioli, P. Alonso-Gonzalez, S. Thongrattanasiri, F. Huth, J. Osmond, M. Spasenovic, A. Centeno, A. Pesquera, P. Godignon, A. Z. Elorza, N. Cama, F. J. G. Abajo, R. Hillenbrand, and F. H. L. Koppens. *Nature* **487**, 77 (2012).

[16] J. A. Gerber, S. Berweger, B. T. O'Callahan, and M. B. Raschke. *Phys. Rev. Lett.* **113**, 055502 (2014).

[17] Z. Zheng, J. Li, T. Ma, H. Fang, W. Ren, J. Chen, J. She, Y. Zhang, F. Liu, H. Chen, S. Deng and N. Xu. *Light-Sci. Appl.* **6**, e17057 (2017).

[18] Z. Fei, M. E. Scott, D. J. Gosztola, J. J. Foley, J. Yan, D. G. Mandrus, H. Wen, P. Zhou, D. W. Zhang, Y. Sun, J. R. Guest, S. K. Gray, W. Bao, G. P. Wiederrecht, and X. Xu. *Phys. Rev. B* **94**, 081402 (2016).

[19] F. Hu, Y. Luan, M. E. Scott, J. Yan, D. G. Mandrus, X. Xu, and Z. Fei. *Nat. Photonics* **11**, 356 (2017).

[20] D. Hu, X. Yang, C. Li, R. Liu, Z. Yao, H. Hu, S. N.

Gilbert Corder, J. Chen, Z. Sun, M. Liu, and Q. Dai. *Nat. Commun.* **8**, 1471 (2017).

[21] P. Li, I. Dolado, F. J. Alfaro-Mozaz, F. Casanova, L. E. Hueso, S. Liu, J. H. Edgar, A. Y. Nikitin, S. Vélez, and R. Hillenbrand. *Science* **359**, 892 (2018).

[22] G. Álvarez-Pérez, Kirill Voronin, Valentyn Volkov, Pablo Alonso-González, and A. Y. Nikitin. *Phys. Rev. B* **100**, 235408 (2019).

[23] K. E. Ballantine, J. F. Donegan, and P. R. Eastham. *Phys. Rev. A* **90**, 013803 (2014).

[24] S. Qu, H. Liu, L. Dong, L. Wu, C. Ma, and S. Wang. *Crystals* **7**, 49 (2017).